Optical and Quantum Electronics manuscript No.
(will be inserted by the editor)

Transverse Structure Optimization of Distributed Feedback and Distributed Bragg Reflector Lasers with Surface Gratings

Topi Uusitalo · Heikki Virtanen · Mihail Dumitrescu

Received: date / Accepted: date

Abstract Two figures of merit for single transverse mode operation and an accurate procedure for calculating the coupling coefficient in distributed feedback lasers with laterally-coupled ridge-waveguide surface grating structures and in distributed Bragg reflector lasers with etched-through-ridge-waveguide surface gratings are introduced. Based on the difference in optical confinement between the pumped and un-pumped regions in the transverse plane, the single transverse mode operation figures of merit are effective and easy to calculate, while the improved coupling coefficient calculation procedure gives experimentally confirmed better results than the conventional calculation approaches, particularly for surface gratings with variable refractive index in the grating areas.

Keywords surface gratings · single transverse mode operation · grating coupling coefficient

1 Introduction

Single transverse mode (STM) and single longitudinal mode (SLM) operation are essential laser characteristics for a broad range of applications ranging from optical communications to atomic clocks. The fabrication of conventional buried-grating distributed feedback (DFB) and distributed Bragg reflector (DBR) lasers requires two or more epitaxial growth steps. Removing the epiwafer from the molecular beam epitaxy reactor, processing the gratings, cleaning the processed surface and overgrowing the structure with the remaining top epilayer structure is a complicated fabrication process, which affects the device performance, decreases the fabrication yield and reduces device reliability, ultimately increasing the device cost. The reduction in reliability is mainly due to the fact that the defect-prone processed interfaces are placed in regions with high operating temperatures and

The research has been done within the European Space Agency ESA project Submegahertz Linewidth Laser for Fundamental Physics Missions (contract No. 4000110645/13/NL/HB).

T. Uusitalo · H. Virtanen · M. Dumitrescu
ORC, Tampere University of Technology, P.O. Box 692, FIN-33101 Tampere, Finland
E-mail: topi.uusitalo@tut.fi

they interact strongly both with the carrier flow and with a high-intensity optical field (the buried gratings must be placed in regions with high optical field intensity in order to achieve good grating coupling coefficient values because they have small refractive index contrast in the grating area).

Employing laterally-coupled ridge-waveguide (LC-RWG) surface gratings for DFB lasers and etched-through-ridge-waveguide (ET-RWG) surface gratings for DBR lasers avoids the problematic over-growth and enables the use of simple epilayer structures. The LC-RWG and ET-RWG surface gratings, illustrated in Fig. 1, are fabricated, without regrowth, on the complete/final epilayer structure, are applicable to different semiconductor materials and can be easily integrated in complex device structures without requiring a difficult epitaxial growth and fabrication process. The surface gratings can achieve a relatively high grating coupling coefficient without being placed in regions with high optical field intensity, due to the fact that they have a high optical contrast in the grating area. They are also placed somehow away from the laser regions with the highest temperature and imply a negligible interaction between the defect-prone processed grating interfaces and the carriers. All these characteristics of LC-RWG and ET-RWG surface gratings lead to more stable devices with better performances and increased reliability.

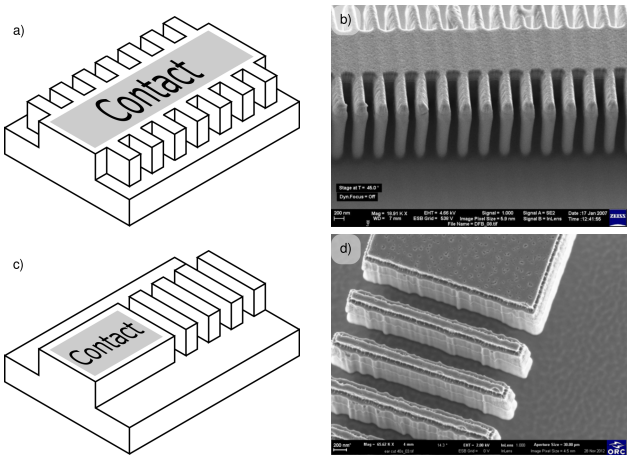

Fig. 1 Sketches a), c) and SEM pictures b), d) of a laterally-coupled ridge-waveguide DFB grating and of an etched-through-ridge-waveguide DBR grating, respectively

The STM operation is determined by the transverse modal gain discrimination (Laakso et al, 2008) and by the difference between the grating coupling coefficients of the transverse modes. A high modal gain in ridge waveguide lasers is ensured by having a high under-the-ridge optical confinement factor (i.e. by having a high confinement of the transverse optical field distribution in the electrically pumped areas, which are under the ridge contact). Unfortunately, for LC-RWG (but less for ET-RWG) surface gratings a high under-the-ridge optical confinement factor implies reduced optical confinement factor in the grating areas and, hence, a reduced grating coupling coefficient (κ). Moreover, since the higher-order transverse

modes are generally less confined transversely, they have a higher presence in the surface grating areas and thus have a higher grating coupling coefficient than the fundamental mode.

The proposed calculation procedures extend on previous work (Laakso et al, 2008), but neglect effects such as radiating waves, which have an effect on the effective coupling coefficient (Millett et al, 2008). However, simplifying the model enables a fast investigation over a large solution space in search of the range of transverse structure dimensions that lead to the highest modal gain advantage for the fundamental mode while also providing a high enough grating coupling coefficient κ between the forward and backward propagating waves. In other work the effect of grating depth on κ has been considered (Wang et al, 2005), but STM operation is usually neglected and only certain structural parameters are considered.

2 Calculation Procedures

2.1 Transverse Mode Discrimination

The transverse mode gain discrimination is given by the modal gain difference between the fundamental mode and higher-order modes. The magnitude of the modal gain G_m for the m$^{\text{th}}$ transverse mode is determined by the convolution of the transverse distribution of the material gain $g(x, y)$ and the transverse optical field intensity distribution of the m$^{\text{th}}$ mode $\Psi_m^2(x, y)$ (Mroziewicz et al, 1991):

$$G_m = \frac{\iint \Psi_m^2(x, y) \cdot g(x, y)\, dx\, dy}{\iint \Psi_m^2(x, y)\, dx\, dy}. \tag{1}$$

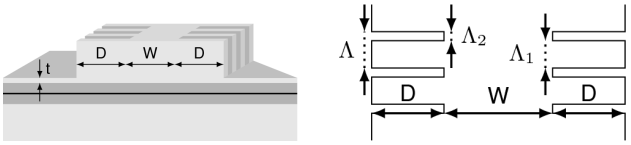

Fig. 2 Schematic 3D and top views of a LC-RWG grating. W: ridge width; D: flange lateral extension; t: remaining un-etched cladding layer thickness; Λ: grating period; Λ_1: flange width; Λ_2: trench width

Good approximate transverse optical field distributions for the guided modes can be obtained with a Mode Solver applied to the longitudinally-averaged transverse distribution of the refractive index. Using longitudinal averaging of the refractive index transverse distribution is based on the continuity conditions at the interfaces between grating slices and on the longitudinal periodicity of the optical field variation, and assumes that the length of the grating period is comparable with the wavelength. The longitudinal averaging is a valid approximation particularly when the perturbation induced by the grating to the effective refractive index of the propagating modes is small, which is generally true for surface gratings, due to the limited confineent of the optical field in the grating area. The

weighted average has been used previously both in the transverse plane solutions (Alman et al, 1992) and in the longitudinal direction averaging (Chen et al, 1996; Jerry et al, 1996). The longitudinal averaging approximation has been indirectly confirmed by the fitting between the experimental emission wavelengths and the effective refractive index values calculated using the longitudinal averaging. The longitudinal averaging simplifies the calculations, contributing to faster scanning of a large structural parameter space. In a LC-RWG grating with rectangular lateral corrugations (like in Fig. 2) the longitudinally-averaged transverse refractive index distribution is obtained from the transverse refractive index distributions in the successive wide-ridge and narrow-ridge grating slices:

$$n_{\mathrm{avg}}(x,y) = \sqrt{\gamma \cdot n^2_{\mathrm{wide}}(x,y) + (1-\gamma) \cdot n^2_{\mathrm{narrow}}(x,y)} \tag{2}$$

where γ is the grating filling factor ($\gamma = \Lambda_1/\Lambda$ from Fig. 2), n_{avg}, n_{wide} and n_{narrow} are the transverse distributions of the longitudinally-averaged refractive index and of the refractive index in the wide (W+2D) ridge and narrow (W) ridge grating slices, respectively.

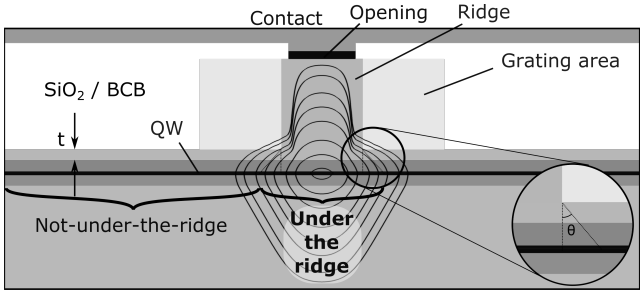

Fig. 3 Schematic cross-section of a LC-RWG grating with a field intensity distribution illustrated with log-spaced contour lines. QW: quantum well

Since the local material gain distribution cannot be evaluated without significant computational effort, we have employed two different approximations for the material gain distribution that enable a fast evaluation of the transverse modal gain discrimination. The first approximation assumes that the local material gain is constant and positive ($g(x,y) = g$) in the pumped active region under-the-ridge and contact and zero elsewhere. This step gain approximation assumes a step lateral distribution of the current in the active region and non-absorbing high-bandgap material outside the pumped area in all regions where the optical field intensity is non-negligible. Under this step gain approximation the modal gain for the m$^{\mathrm{th}}$ transverse mode is given by:

$$G_m = g \frac{\iint\limits_{\text{active region, under-the-ridge}} \Psi_m^2(x,y)\,dx\,dy}{\iint\limits_{-\infty}^{+\infty} \Psi_m^2(x,y)\,dx\,dy} = g\Gamma_m^+, \tag{3}$$

where Γ_m^+ is the under-the-ridge active region confinement factor for the m$^{\mathrm{th}}$ transverse mode.

The step gain approximation is suited for deeply etched LC-RWG structures since deep etching close to the active region implies a limited lateral current diffusion. Also, since the absorbing regions outside the pumped area affect the higher order modes more, this approximation is more likely to give a false negative than a false positive STM evaluation. Moreover, the lateral current diffusion can be taken into account by extending the pumped active region area laterally, beyond the region placed strictly under the ridge and contact.

According to the step gain approximation, a stable STM-operation is associated with the maximization of all the ratios of the following type:

$$\Gamma_{1m}^{+} = \frac{g\Gamma_1^{+} - g\Gamma_m^{+}}{g\Gamma_1^{+}} = \frac{\Gamma_1^{+} - \Gamma_m^{+}}{\Gamma_1^{+}}. \tag{4}$$

Since Γ_2^+ is generally bigger than Γ_4^+, Γ_6^+, ... and Γ_3^+ is generally bigger than Γ_5^+, Γ_7^+, ..., a good STM-operation figure of merit under the step gain approximation can be derived just from ratios Γ_{12}^+ and Γ_{13}^+:

$$\begin{aligned} \Gamma_{123}^{+} = \Gamma_{12}^{+} \cdot \Gamma_{13}^{+} &= \frac{\Gamma_1^{+} - \Gamma_2^{+}}{\Gamma_1^{+}} \cdot \frac{\Gamma_1^{+} - \Gamma_3^{+}}{\Gamma_1^{+}} \\ &= \frac{\left(\Gamma_1^{+} - \Gamma_2^{+}\right) \cdot \left(\Gamma_1^{+} - \Gamma_3^{+}\right)}{(\Gamma_1^{+})^2} \end{aligned} \tag{5}$$

Because in many instances the higher-order mode loss is an important factor, a STM operation figure of merit that also takes into account the loss discrimination could be more effective. Such a gain-loss STM figure of merit can be derived from the approximation that the constant gain in the under-the-ridge pumped area of the active region is equal with the constant absorption loss in the un-pumped area of the active region and zero elsewhere. The step gain-loss approximation can be refined by adjusting the switching point between gain and loss regions such that the approximated modal gain fits the modal gain calculated with an accurate method. With this step gain-loss approximation, the modal gain for the m^{th} transverse mode (1) can be simplified to:

$$G_m = g\Gamma_m^{\pm} = g\Gamma_m^{+} - g\Gamma_m^{-}, \tag{6}$$

where Γ_m^+ and Γ_m^- are the "under-the-ridge" and "not-under-the-ridge" optical confinement factors for the m^{th} transverse mode in the pumped and un-pumped active region areas, respectively.

The modal gain-loss discrimination figure of merit for achieving STM operation is associated with a high gain-loss difference between the fundamental mode and any higher order mode:

$$\begin{aligned} G_1 - G_m &= g \cdot (\Gamma_1^{+} - \Gamma_1^{-}) - g \cdot (\Gamma_m^{+} - \Gamma_m^{-}) \\ &= g \cdot (\Gamma_1^{+} - \Gamma_m^{+}) + g \cdot (\Gamma_m^{-} - \Gamma_1^{-}) \end{aligned} \tag{7}$$

Because the fundamental mode is better confined in the active region under-the-ridge while higher order modes have higher confinement in the active region

not under-the-ridge, the gain-loss discrimination figure of merit between the fundamental mode and the m$^{\text{th}}$ mode can be normalized according to:

$$\begin{aligned} \Gamma_{1m}^{\pm} &= \frac{g\Gamma_1^+ - g\Gamma_m^+}{g\Gamma_1^+} + \frac{g\Gamma_m^- - g\Gamma_1^-}{g\Gamma_m^-} \\ &= \frac{\Gamma_1^+ - \Gamma_m^+}{\Gamma_1^+} + \frac{\Gamma_m^- - \Gamma_1^-}{\Gamma_m^-}. \end{aligned} \tag{8}$$

Moreover, since the second mode is generally better confined in the active region under-the-ridge and less confined in the active regions not under-the-ridge as compared with higher-order even modes, while a similar situation is encountered in the comparison between the third mode and higher-order odd modes, the gain-loss figure of merit for STM operation can be evaluated by studying the normalized product of $\Gamma_{12}^{\pm}$ and $\Gamma_{13}^{\pm}$:

$$\Gamma_{123}^{\pm} = \left(\Gamma_{12}^{\pm} \cdot \Gamma_{13}^{\pm}\right) \cdot \frac{1}{4}, \tag{9}$$

where division by 4 is used for normalization because each summand in Eq. (8) has a maximum value of 1 and thus each factor in Eq. (9) has a maximum value of 2. The normalization enables the comparison of the STM gain-loss figures of merit for different structures.

It should be noted that the two modal gain discrimination figures of merit, Γ_{123}^{+} and $\Gamma_{123}^{\pm}$, are not based on accurate calculations of the modal gains but rather on good enough evaluations of the modal gain ratios between the fundamental and higher order modes. The good evaluation of the modal gain ratios is based on the fact that the employed approximations affect all modal gains in a similar way.

2.2 Grating coupling coefficient evaluation

An accurate evaluation of the coupling coefficient (κ) is essential for designing DFB and DBR lasers. Generally the coupling coefficient for the m$^{\text{th}}$ transverse mode (κ_m) can be evaluated from the expression (Streifer et al, 1975):

$$\kappa_m = \frac{k_0^2}{2\beta_m} \frac{\iint \Delta\epsilon(x,y)\Psi_{\text{m}}(x,y)^2\, dx\, dy}{\iint \Psi_{\text{m}}(x,y)^2\, dx\, dy}, \tag{10}$$

where the integration is carried out over the whole (x,y)-plane, Ψ_{m} is the m$^{\text{th}}$ transverse mode optical field distribution for the longitudinally averaged transverse refractive index distribution, and $\Delta\epsilon$ is the perturbation in the dielectric constant. For the o$^{\text{th}}$ order rectangular gratings the perturbation term is (Agraval and Dutta, 1993):

$$\Delta\epsilon_o(x,y) = \left(n_2(x,y)^2 - n_1(x,y)^2\right) \cdot \frac{\sin(\pi o\gamma)}{\pi o}, \tag{11}$$

where $n_1(x,y)$ and $n_2(x,y)$ are the transverse refractive index distributions in the longitudinally alternating grating slices. It should be noted that the coupling coefficient formula is based on small-signal analysis, and the longitudinal perturbation of the effective dielectric constant (which is derived from the convolution

of $\Delta\epsilon$ with the optical field intensity distribution) should always be much smaller than the average values of the effective dielectric constants in different longitudinal parts of the grating. Combining equations 10 and 11 yields:

$$\kappa_m = \frac{k_0}{2n_{\mathrm{eff,m}}} \frac{\iint \left(n_2(x,y)^2 - n_1(x,y)^2\right) \Psi_{\mathrm{m}}(x,y)^2 \, dx \, dy}{\iint \Psi_{\mathrm{m}}(x,y)^2 \, dx \, dy} \cdot \frac{\sin(\pi o \gamma)}{\pi o}, \tag{12}$$

where $n_{\mathrm{eff,m}}$ is the effective refractive index corresponding to the m^{th} transverse mode, calculated for the longitudinally averaged transverse refractive index distribution.

Because outside the grating area $n_2(x,y)^2 - n_1(x,y)^2 = 0$ and under the assumption that the refractive index distributions are constant in the grating areas of the grating slices ($n_1(x,y) = n_1$ and $n_2(x,y) = n_2$ in the grating areas), the standard formula for the rectangular grating coupling coefficient results as:

$$\kappa_m = \frac{k_0}{2n_{\mathrm{eff,m}}} \cdot (n_2^2 - n_1^2) \cdot \Gamma_{\mathrm{g,m}} \cdot \frac{\sin(\pi o \gamma)}{\pi o} \tag{13}$$

where o is the grating order and $\Gamma_{\mathrm{g,m}}$ is the optical confinement factor of the m^{th} transverse mode in the grating area.

An approximation which assumes that $n_1 + n_2 \approx 2 \cdot n_{\mathrm{eff,m}}$ is frequently used in combination with the standard formula:

$$\kappa_m \approx \frac{2 \cdot (n_2 - n_1)}{\lambda_0} \cdot \Gamma_{\mathrm{g,m}} \cdot \frac{\sin(\pi o \gamma)}{o}. \tag{14}$$

This approximation is valid for conventional buried gratings, since for them the alternating grating materials are semiconductors with refractive index values close to $n_{\mathrm{eff,m}}$. However, for the surface grating structures this approximation overestimates κ_m, because $n_1 + n_2 < 2 \cdot n_{\mathrm{eff,m}}$ as one of the alternating grating materials is a dielectric with much lower refractive index but a small influence on $n_{\mathrm{eff,m}}$. A better calculation approach for the grating coupling coefficient, which does not assume constant refractive index distributions in the grating areas of the grating slices and is valid for all types of gratings, employs the effective refractive index values for the two successive slices of the grating, $n_{\mathrm{eff,m:2}}$ and $n_{\mathrm{eff,m:1}}$:

$$\begin{aligned} \kappa_m &= \frac{k_0}{2n_{\mathrm{eff,m}}} \left(\frac{\iint n_2(x,y)^2 \Psi_{\mathrm{m}}(x,y)^2 \, dx \, dy}{\iint \Psi_{\mathrm{m}}(x,y)^2 \, dx \, dy} - \right. \\ &\quad \left. \frac{\iint n_1(x,y)^2 \Psi_{\mathrm{m}}(x,y)^2 \, dx \, dy}{\iint \Psi_{\mathrm{m}}(x,y)^2 \, dx \, dy} \right) \cdot \frac{\sin(\pi o \gamma)}{\pi o} \\ &= \frac{k_0}{2n_{\mathrm{eff,m}}} \left(n_{\mathrm{eff,m:2}}^2 - n_{\mathrm{eff,m:1}}^2 \right) \cdot \frac{\sin(\pi o \gamma)}{\pi o}. \end{aligned} \tag{15}$$

The effective refractive index values corresponding to the grating slices ($n_{\mathrm{eff,m:2}}$ and $n_{\mathrm{eff,m:1}}$) cannot be calculated directly with a Mode Solver applied to the refractive distributions of the grating slices because this would imply boundary condition violations in the longitudinal direction. A good approximate effective refractive index calculation procedure for the grating slices is to use the convolution of the

transverse optical field distribution ($\Psi_{\mathrm{m}}(x,y)$), obtained for the longitudinally-averaged transverse refractive index distribution, with the transverse refractive index distributions in the grating slices, which leads to:

$$n^2_{\mathrm{eff,m:slice}} = \frac{\iint \Psi^2_{\mathrm{m}} \cdot n^2_{\mathrm{slice}}\, dx\, dy}{\iint \Psi^2_{\mathrm{m}}\, dx\, dy} - \frac{\iint \left(\nabla\Psi_{\mathrm{m}}\right)^2\, dx\, dy}{k_0^2 \cdot \iint \Psi^2_{\mathrm{m}}\, dx\, dy}. \tag{16}$$

This corresponds also to the derivation of the κ formula from coupled mode theory (Dutta and Agrawal, 1993; Streifer et al, 1975) because the second term on the right hand side of Eq. (16) is canceled in the effective refractive index contrast of Eq. (15).

3 Results and Discussion

A comparison between the step gain approximation and the improved step gain-loss approximation STM figures of merit can be made by comparing Fig. 4 with Fig. 5, where both figures of merit are plotted as a function of un-etched cladding thickness (t) and ridge width (W) for different supplementary lateral extensions of the "under-the-ridge" gain active area beyond the region strictly under the ridge (as defined by the angle θ of lateral current divergence in the epilayer below the etching depth, shown in the inset of Fig. 3).

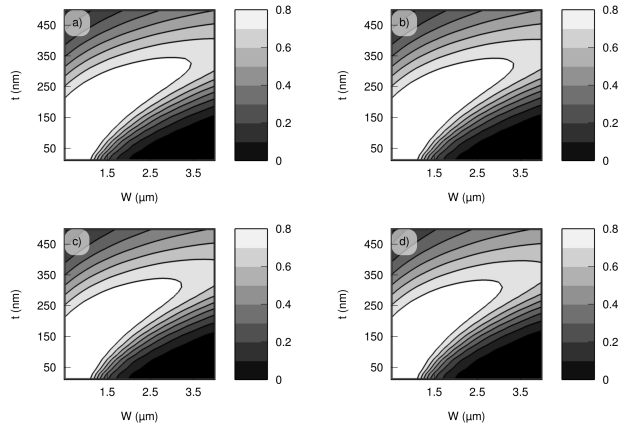

Fig. 4 Variation of the STM figure of merit Γ^+_{123} as a function of ridge width (W) and un-etched cladding thickness (t) for different lateral current divergence angles below the etching depth level θ: a) $\theta = 0°$, b) $\theta = 15°$, c) $\theta = 30°$, d) $\theta = 45°$

The structure for which the calculations have been done is a LC-RWG grating designed for 780 nm operation with D=2.5 μm. From both Fig. 4 and Fig. 5 it can be seen that the supplementary lateral extension of the "under-the-ridge" active area does not influence significantly the figures of merit as long as the extension does not exceed a value corresponding to the epilayer thickness between the grating etching depth level and the active region depth level.

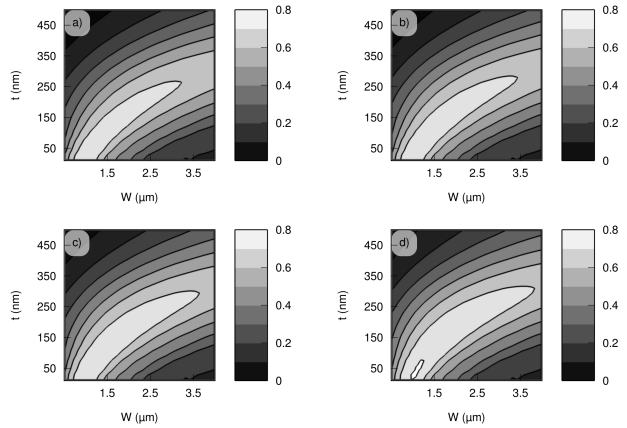

Fig. 5 Variation of the STM figure of merit $\Gamma_{123}^{\pm}$ as a function of ridge width (W) and unetched cladding thickness (t) for different lateral current divergence angles below the etching depth level θ: a) $\theta = 0°$, b) $\theta = 15°$, c) $\theta = 30°$, d) $\theta = 45°$

The comparison between Fig. 4 and Fig. 5 shows that the step gain-loss figure of merit gives a narrower range of transverse dimensions for the best STM operation. The parameter combinations that correspond to a good/stable STM operation are the ones that maximize the two figures of merit, but the absolute values of the two different figures of merit, Γ_{123}^{+} and $\Gamma_{123}^{\pm}$, are not directly comparable.

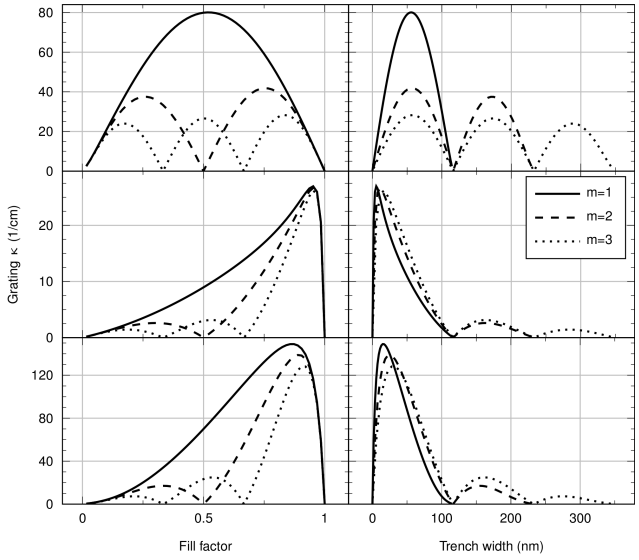

Fig. 6 Comparison of κ variation as a function of grating filling factor (left panels) and grating trench width (right panels) for three different structures. Top panels: buried grating; middle panels: LC-RWG surface grating with W = 2.0 μm, D = 2.5 μm and t = 150 nm; bottom panels: ET-RWG surface grating with W = 2.0 μm and t = 150 nm. In each panel the solid line is for a first, the dashed line is for a second and the dotted line is for a third order grating

Fig. 6 gives the variation of κ as a function of the grating filling factor γ and as a function of the grating trench width for three different grating structures. The buried grating κ changes symmetrically below and above 0.5 filling factor, because the filling factor doesn't change the transverse optical field profile considerably. However, the variation of κ with the filling factor is strongly asymmetrical for the surface gratings. This is due to the fact that a change in the filling factor of the surface gratings induces a significant change in the transverse optical field profile, which affects the confinement factor in the grating area and the effective refractive indexes of the alternating slices. The dependencies of the grating coupling coefficient on the grating trench width, given in right panels of Fig. 6, illustrate that, due to the particular interaction of the surface gratings with the optical field, a high surface grating coupling coefficient is obtained for narrow grating trenches irrespective of the grating order.

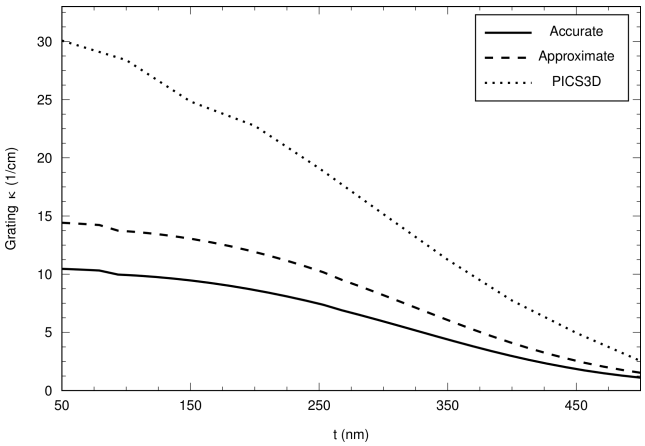

Fig. 7 Comparison of κ variation as a function of un-etched cladding thickness, calculated with different procedures for a 1st-order LC-RWG grating with W = 2.0 µm, D = 2.5 µm and γ=0.5. The solid line has been obtained using Eq. (15), the dashed line has been obtained using the approximate Eq. (14), and the dotted line has been obtained by using PICS3D (Crosslight Software Inc., 2005) (version 2006.11.01)

The coupling coefficient value dependencies on the un-etched cladding thickness calculated for a 1st-order LC-RWG grating with W = 2.0 µm, D = 2.5 µm and γ=0.5, using Eq. (15), using the approximate Eq. (14) and using PICS3D are compared in Fig. 7. The difference between the experimentally confirmed values calculated with Eq. (15) and the values calculated with Eq. (14) are due to the approximation $n_1 + n_2 \approx 2 \cdot n_{\text{eff}}$, which leads to an over-estimation of κ by Eq. (14). PICS3D also uses the approximate Eq. (14), and the supplementary over-estimation is due to the fact that the values calculated by Eq. (14) are dependent on the very small value of the optical confinement factor in the grating region, which is very sensitive to mesh variations. The calculations performed with Eq. (15) do not imply any approximations, are more robust with respect to mesh variations and provide the effective refractive index values for the grating slices, which can be used in longitudinal transfer matrix simulations.

4 Conclusions

Two figures of merit facilitating single transverse mode (STM) operation evaluation based on step gain and on step gain-loss distribution approximations have been introduced. The figures of merit are easy to calculate and enable a fast evaluation of STM operation over a broad range of transverse structural parameters. The figure of merit based on the step gain-loss distribution approximation gives narrower ranges for the transverse structural parameters that lead to STM operation and has been confirmed by numerous experiments with various RWG and LC-RWG structures operating at different wavelengths.

The proposed coupling coefficient calculation does not imply the approximations used in the standard formulas, is applicable to grating structures with variable refractive index across the grating area of the grating slices, is more accurate and more robust to mesh variations, particularly for surface gratings.

References

Agraval GP, Dutta NK (1993) Semiconductor Lasers. Springer US

Alman GM, Molter LA, Shen H, Dutta M (1992) Refractive index approximations from linear perturbation theory for planar mqw waveguides. IEEE journal of quantum electronics 28(3):650–657

Chen C, Chen L, Wang Q, et al (1996) Coupling coefficients of gain-coupled distributed feedback lasers with absorptive grating

Crosslight Software Inc (2005) Crosslight Software | PICS3D

Dutta NK, Agrawal G (1993) Semiconductor lasers

Jerry C, Clifton G, et al (1996) Evaluation of coupling coefficients for laterally-coupled distributed feedback lasers. Japanese journal of applied physics 35(9R):4654

Laakso A, Dumitrescu M, Pietilä P, Suominen M, Pessa M (2008) Optimization studies of single-transverse-mode 980 nm ridge-waveguide lasers. Optical and quantum electronics 40(11-12):853–861

Millett RR, Hinzer K, Hall TJ, Schriemer H (2008) Simulation analysis of higher order laterally-coupled distributed feedback lasers. IEEE Journal of Quantum Electronics 44(12):1145–1151

Mroziewicz B, Bugajski M, Nakwaski W (1991) Physics of semiconductor lasers

Streifer W, Scifres DR, Burnham RD (1975) Coupling coefficients for distributed feedback single-and double-heterostructure diode lasers. Quantum Electronics, IEEE Journal of 11(11):867–873

Wang J, Tian JB, Cai PF, Xiong B, Sun CZ, Luo Y (2005) 1.55-/spl mu/m algainas-inp laterally coupled distributed feedback laser. IEEE photonics technology letters 17(7):1372–1374